

Phase diagram of Fe-doped Ni-Mn-Ga ferromagnetic shape-memory alloys

Daniel Soto, Francisco Alvarado Hernández, Horacio Flores
*Centro de Investigaciones en Materiales Avanzados,
 Miguel de Cervantes 120, Chihuahua, México C. P. 31109.*

Xavier Moya, Lluís Mañosa, Antoni Planes*
*Departament d'Estructura i Constituents de la Matèria, Facultat de Física,
 Universitat de Barcelona, Diagonal 647, E-08028 Barcelona, Catalonia, Spain*

Seda Aksoy, Mehmet Acet
Fachbereich Physik, Experimentalphysik, Universität Duisburg-Essen, D-47048 Duisburg, Germany

Thorsten Krenke
ThyssenKrupp Electrical Steel GmbH, D-45881 Gelsenkirchen, Germany
 (Dated: April 8, 2008)

We have studied the effect of Fe addition on the structural and magnetic transitions in the magnetic shape memory alloy Ni-Mn-Ga by substituting systematically each atomic species by Fe. Calorimetric and AC susceptibility measurements have been carried out in order to study the magnetic and structural transformation properties. We find that the addition of Fe modifies the structural and magnetic transformation temperatures. Magnetic transition temperatures are displaced to higher values when Fe is substituted into Ni-Mn-Ga, while martensitic and premartensitic transformation temperatures shift to lower values. Moreover, it has been found that the electron per atom concentration essentially governs the phase stability in the quaternary system. However, the observed scaling of transition temperatures with e/a differs from that reported in the related ternary system Ni-Mn-Ga.

PACS numbers: 81.30.Kf, 75.50.Cc

I. INTRODUCTION

Magnetic shape-memory alloys have drawn much attention in recent years owing to their unique magnetomechanical properties such as magnetic shape-memory [1] and the magnetic superelasticity [2]. These properties are a consequence of a strong coupling between magnetic and structural degrees of freedom. The prototypical and first discovered magnetic shape-memory material is the Heusler Ni_2MnGa [3]. This alloy undergoes a complex multi-stage transformation process from a high temperature paramagnetic cubic phase to a ferromagnetic martensitic phase. At intermediate temperatures it shows precursor tweed textures which may lock (via a first-order phase transition) into a modulated premartensitic structure due to the freezing of a specific phonon with a given wave vector. This behavior appears to be related to low resistance against distortions of the $\{110\}$ planes along the $\langle 1\bar{1}0 \rangle$ directions and is evidenced by the features of the low energy TA_2 acoustic phonon branch [4, 5, 6, 7] and the low value of the elastic constant C' [8, 9, 10]. While these features are essentially inherent to the high-temperature cubic structure, additional softening has been shown to arise from the coupling between structural and magnetic degrees of free-

dom [6, 7]. Thus, it has been suggested that the magnetostructural coupling is responsible for the phonon condensation yielding the intermediate modulated structure [11]. Nevertheless, the occurrence of a premartensitic phase is not yet a well understood phenomenon, as it only has been observed for a restricted number of magnetic shape memory alloys within limited composition ranges. Actually, the study of the structural (martensitic and premartensitic transformations) and magnetic properties of Ni-Mn-Ga alloys is a current topic of intense research [12, 13, 14, 15, 16, 17, 18].

The effect of doping elements on the martensitic and magnetic transformations in Ni-Mn-Ga alloys has received considerable attention [19, 20, 21, 22, 23, 24, 25]. However, the lack of a systematic study makes it difficult to compare directly the properties of different compounds. In the present paper, we investigate the dependence of transition temperatures (martensitic, intermediate and Curie) on the electron concentration by analyzing the effect of substituting Ni, Mn and Ga by Fe. In all cases, the reference system is the stoichiometric Ni_2MnGa , which has a high temperature L2_1 structure ($Fm\bar{3}m$). This structure can be viewed as four interpenetrating fcc sublattices [in Wickoff notation, (4a)-1 is occupied by Mn-atoms, (4b)-2 by Ga-atoms, and (8c) by Ni-atoms]. The total magnetic moment is $\sim 4.1\mu_B$ per formula unit and is largely confined to the Mn-sites contributing with $3.5\mu_B$.

*Electronic address: toni@ecm.ub.es

TABLE I: Compositions of the Ni-Mn-Ga-Fe samples determined by EDX. Different specimens are grouped into three distinct families, depending on the element that is substituted by Fe (elements within parenthesis, first column). The estimated error in the compositions is less than $\pm 0.3\%$. Values of valence electron concentration per atom, e/a , are also given.

Family	Ni (at. %)	Mn (at. %)	Ga (at. %)	Fe (at. %)	e/a
(Ni,Fe)	52.6	23.1	24.3	0 ^a	7.606
	51.3	22.8	24.5	1.4	7.573
	50.1	23.1	24.6	2.2	7.541
	49.3	23.1	24.5	3.1	7.530
	48.1	23.0	24.5	4.4	7.507
(Mn,Fe)	47.0	23.1	24.6	5.3	7.479
	51.4	24.8	23.8	0 ^b	7.589
	51.5	24.2	23.5	0.8	7.613
	51.1	24.6	23.4	0.9	7.606
	51.7	23.1	23.4	1.8	7.633
(Ga,Fe)	51.3	24.0	24.7	0 ^c	7.551
	51.2	24.2	23.8	0.8	7.592
	51.8	24.8	21.7	1.7	7.703
	51.3	24.5	22.2	2.0	7.671

^aData extracted from reference [26].

^bData extracted from reference [27]. Note that this composition slightly deviates (more than the experimental error, $\pm 0.3\%$) from the fitted compositional line.

^cData extracted from reference [28]. Note that this composition slightly deviates (more than the experimental error $\pm 0.3\%$) from the fitted compositional line.

II. EXPERIMENTAL

Polycrystalline Ni-Mn-Ga-Fe ingots were prepared by arc melting pure metals under argon atmosphere in a water cooled Cu crucible. The ingots were melted several times for homogeneity and encapsulated under vacuum in quartz glass. They were then annealed at 1073 K for 72 hours to achieve a high degree of atomic order. Finally, the samples were quenched in ice-water. The compositions of the alloys were determined by energy dispersive x-ray photoluminescence analysis (EDX) with an estimated error less than $\pm 0.3\%$ (Table I). The alloys are grouped according to their compositions into the families $\text{Ni}_{52.5-x}\text{Mn}_{23}\text{Ga}_{24.5}\text{Fe}_x$ ($1.2 \leq x \leq 5.5$) for which Ni is replaced by Fe; $\text{Ni}_{51.4}\text{Mn}_{25.2-x}\text{Ga}_{23.4}\text{Fe}_x$ ($0.8 \leq x \leq 1.8$) for which Mn is replaced by Fe; and $\text{Ni}_{51.4}\text{Mn}_{24.5}\text{Ga}_{24.1-x}\text{Fe}_x$ ($0.7 \leq x \leq 2.0$) where Fe replaces Ga. The compositions are given in at%.

Specimens cut from the ingots using a low speed diamond saw (typical size $5 \times 1 \times 1 \text{ mm}^3$) were used as samples for susceptibility and calorimetric studies. Structural transition temperatures were obtained from AC susceptibility and calorimetric measurements. Mag-

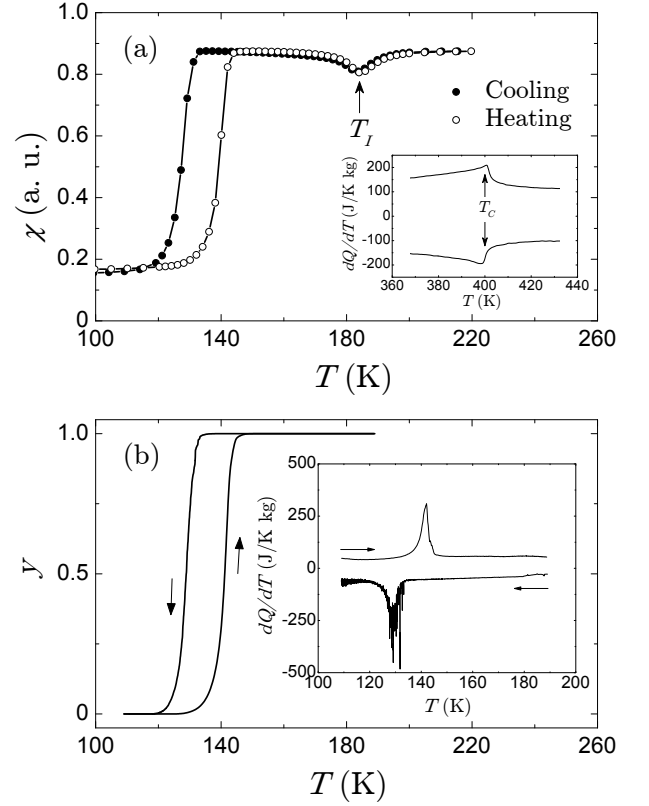


FIG. 1: $\text{Ni}_{52.5-x}\text{Mn}_{23}\text{Ga}_{24.5}\text{Fe}_x$ family represented by the sample with $x = 4.4$. (a) Magnetic susceptibility versus temperature. The vertical arrow indicates the premartensitic transition temperature, T_I . The inset shows high temperature calorimetric curves. The Curie point T_C is indicated by vertical arrows. (b) Transformed fraction as a function of temperature obtained by integration of the calorimetric curves (inset in b). The arrows indicate the direction of temperature change.

netic susceptibility measurements were carried out in an AC susceptometer (LakeShore 7120A) in the temperature range $80 \text{ K} \leq T \leq 320 \text{ K}$. The working parameters were 500 A m^{-1} (6.28 Oe) applied field and 389 Hz frequency. For differential scanning calorimetry (DSC) measurements, one side of the samples was ground with SiC abrasive to ensure optimal thermal contact. Calorimetric measurements were carried out by means of a high sensitivity calorimeter in the temperature range $100 \text{ K} \leq T \leq 350 \text{ K}$. Typical heating and cooling rates were 0.5 K min^{-1} . Magnetic transition temperatures were determined by means of a DSC calorimeter suitable for higher temperatures. All transition temperatures are affected by an error of $\pm 1 \text{ K}$. The errors in entropy change are based on reproducibility and shown as error bars in the figures.

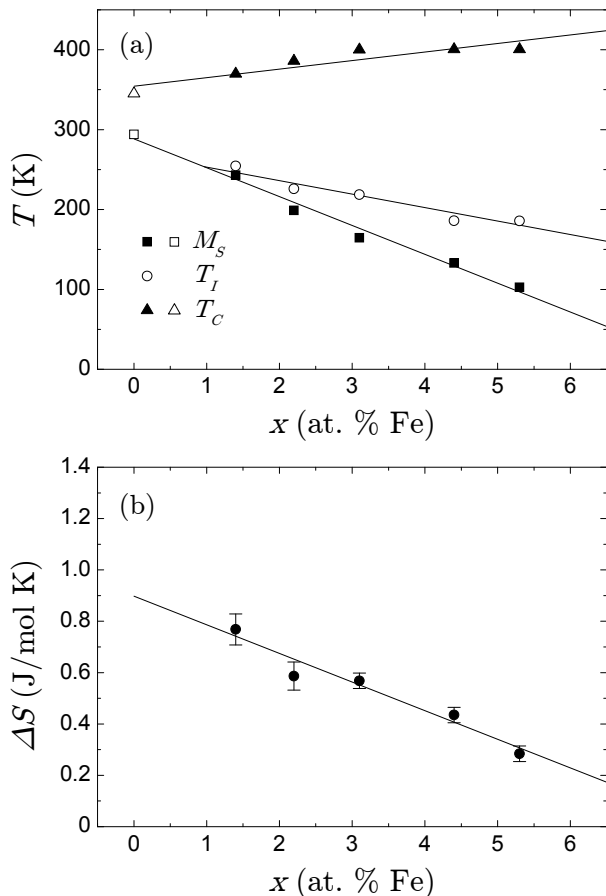


FIG. 2: (a) Evolution of the transition temperatures of $\text{Ni}_{52.5-x}\text{Mn}_{23}\text{Ga}_{24.5}\text{Fe}_x$ as a function of Fe concentration. Open square and triangle symbols stand for data extracted from ref. [26]. (b) Entropy change at the martensitic transformation as a function of Fe concentration. Solid lines are linear fits to the experimental data.

III. EXPERIMENTAL RESULTS

Eleven different alloys were studied in the present work. In this section, we present selected results of susceptibility and calorimetric measurements which are representative of each family. In the following the given Fe content is taken as the value corresponding to the fitted compositional line. From the complete set of data, we determine a phase diagram for each family and the transition entropy change at the martensitic transformation.

A. Substitution of Ni by Fe

Figure 1 shows the AC susceptibility and calorimetric curves for the sample with $x = 4.4$. The inset in figure 1(b) shows the calorimetric curves recorded on cooling and heating. The multiple peaks (noticeable in the thermograms corresponding to the forward transition on cooling) are a consequence of the well-known

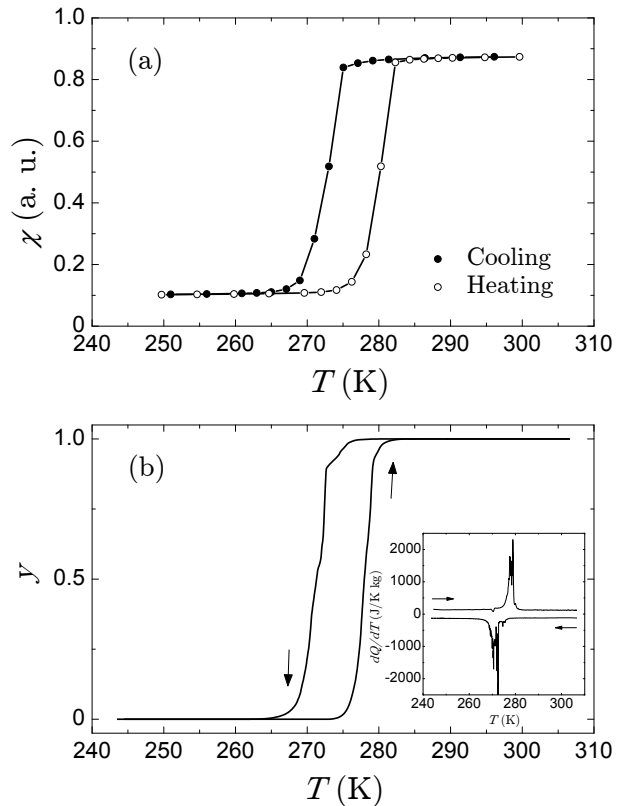


FIG. 3: $\text{Ni}_{51.4}\text{Mn}_{25.2-x}\text{Ga}_{23.4}\text{Fe}_x$ family represented by the sample with $x = 1.8$. (a) Magnetic susceptibility versus temperature and (b) transformed fraction as a function of temperature, obtained by integration of the calorimetric curves (shown in the inset). Arrows in panel (b) and inset indicate direction of temperature change.

jerky character of martensitic transformations. On the other hand, the extra noise observed at the lowest temperatures in the thermograms on cooling is an artifact arising from the very low cooling rate in the low temperature regime (notice that dQ/dT is obtained by dividing the calorimetric signal \dot{Q} by \dot{T}). Figure 1(b) shows the austenitic transformed fraction, y versus T , obtained from the calorimetric data shown in the inset. The austenitic transformed fraction is computed as $y = 1 - \Delta S(T)/\Delta S$ for the forward transition on cooling, and $y = \Delta S(T)/\Delta S$ for the reverse transition on heating, with $\Delta S(T) = \int_{T_i}^T (dQ/dT)/T dT$ ($T < T_i$ on cooling and $T > T_i$ on heating) and ΔS , the entropy change at the martensitic transformation. This plot is illustrative for the typical results obtained for the $\text{Ni}_{52.5-x}\text{Mn}_{23}\text{Ga}_{24.5}\text{Fe}_x$ family. Both susceptibility and calorimetric measurements reveal the presence of a martensitic transformation. The corresponding transition temperatures are: martensite start temperature $M_s = 133$ K, martensite finish temperature $M_f = 119$ K, austenite start temperature $A_s = 132$ K and austenite finish temperature $A_f = 146$ K. The Curie point was determined from complementary DSC measurements as

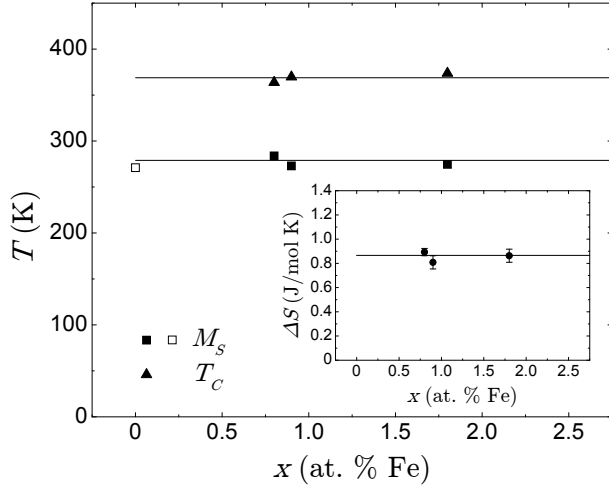


FIG. 4: Transition temperatures for $\text{Ni}_{51.4}\text{Mn}_{25.2-x}\text{Ga}_{23.4}\text{Fe}_x$ as a function of Fe concentration. Open square symbol stands for data extracted from ref. [27], for this sample T_C was not reported. The inset shows the entropy change at the martensitic transformation as a function of Fe concentration. Solid lines are fits to the experimental data.

$T_C = 400$ K [shown in the inset of Fig. 1(a)]. Moreover, an additional feature is observed in the susceptibility curve at temperatures above the martensitic transition which is associated with the formation of the intermediate or premartensitic phase [9]. The transition temperature is $T_I = 186$ K. No significant thermal hysteresis is detected at the premartensitic transition and no appreciable features are observed in the calorimetric curves at the premartensitic transition. This behaviour agrees with that observed in the related system Ni-Mn-Ga, where thermal anomalies are barely detected with differential scanning calorimetric techniques [29]. By contrast, AC susceptibility measurements are very suited for the observation of the intermediate phase transition [9].

Figure 2(a) summarizes the results for the $\text{Ni}_{52.5-x}\text{Mn}_{23}\text{Ga}_{24.5}\text{Fe}_x$ family. To complete the picture, we have also included data for an $x = 0$ sample from reference [26]. Transition temperatures are plotted as a function of the Fe concentration. All transition temperatures associated with the martensitic transformation (M_s , M_f , A_s and A_f) follow the same x dependence. Thus, for the sake of clarity, only M_s temperatures are included. As can be seen from this figure, the martensitic transformation temperature decreases as the amount of Fe increases. In ternary Ni-Mn- X (X : Ga, Al, Sn, In and Sb) systems it is well established that martensitic transformation temperatures decrease as the valence electron concentration e/a decreases [30, 31, 32, 33]. When replacing Ni by Fe, e/a decreases and a drop in M_s is expected. This behavior is seen in Fig. 2(a).

Premartensitic transformation temperatures also decrease as the Fe concentration increases, but at lower rate than M_s . In addition T_C increases with increasing x .

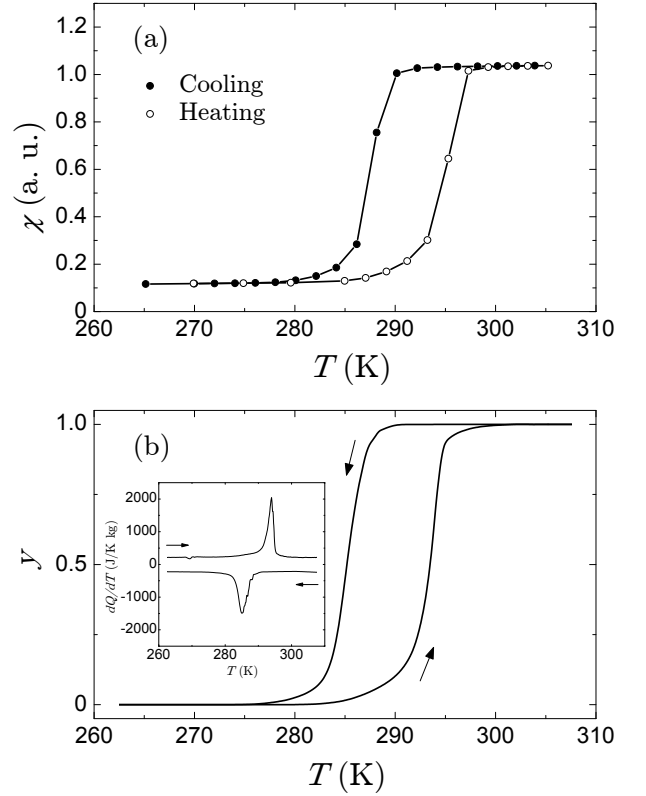


FIG. 5: $\text{Ni}_{51.4}\text{Mn}_{24.5}\text{Ga}_{24.1-x}\text{Fe}_x$ family represented by the sample with $x = 0.7$. (a) Magnetic susceptibility versus temperature and (b) transformed fraction as a function of temperature, obtained by integration of the calorimetric curves (shown in the inset). Arrows in panel (b) and inset indicate direction of temperature change.

Figure 2(b) shows the entropy change at the martensitic transformation as a function of Fe concentration. The concentration dependence of ΔS is similar to the behaviour of M_s , i. e., the entropy change decreases as the amount of Fe increases. Such a dependence reflects the stabilization of the cubic phase.

B. Substitution of Mn by Fe

Figure 3 illustrates typical results obtained when replacing Mn by Fe ($\text{Ni}_{51.4}\text{Mn}_{25.2-x}\text{Ga}_{23.4}\text{Fe}_x$ family). For the sample with $x = 1.8$ ($T_C = 374$ K) a martensitic transition is observed on cooling at $M_s = 275$ K and $M_f = 267$ K. On heating, the reverse transformation takes place at $A_s = 274$ K and $A_f = 281$ K. No signatures of a premartensitic transformation are observed.

The variation of transition temperatures with Fe concentration for this family is collected in Fig. 4. No significant changes in transition temperatures are observed over the compositional range studied. This is because e/a varies little by replacing Mn with Fe in small amounts. Consistently, Fe addition does not substantially modifies the values of the entropy change at the martensitic tran-

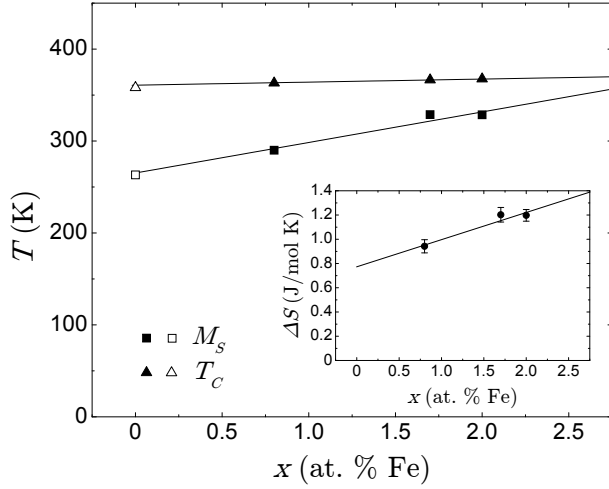


FIG. 6: Transition temperatures for $\text{Ni}_{51.4}\text{Mn}_{24.5}\text{Ga}_{24.1-x}\text{Fe}_x$ as a function of Fe concentration. Open square and triangle symbols stand for data extracted from ref. [28]. The inset shows the entropy change at the martensitic transformation as a function of Fe concentration. Solid lines are linear fits to the experimental data.

sition, as can be seen in the inset of figure 4.

C. Substitution of Ga by Fe

Figure 5 illustrates typical results obtained for the $\text{Ni}_{51.4}\text{Mn}_{24.5}\text{Ga}_{24.1-x}\text{Fe}_x$ family. Data for the sample with $x = 0.7$ ($T_C = 363$ K) are shown. The presence of a martensitic transformation near room temperature is evidenced from both susceptibility and calorimetric measurements. The corresponding transition temperatures are $M_s = 290$ K, $M_f = 281$ K, $A_s = 287$ K and $A_f = 297$ K. Again, no signature of the premartensitic transition is observed.

The phase diagram is shown in figure 6, where it is seen that M_s increases with increasing Fe content. This is consistent with the rapid increase of e/a when Fe is substituted for Ga. T_C is essentially unaffected.

The entropy change at the martensitic transition as a function of Fe concentration is collected in the inset of figure 6. As can be seen from this figure, ΔS parallels the behaviour of the martensitic transformation temperatures and increases as the amount of Fe increases, pointing out the stabilization of the low temperature phase due to Fe substitution.

IV. DISCUSSION

The complete set of results for the different transition temperatures is collected in Fig. 7. Here, the magnetic and structural transition temperatures of the quaternary Ni-Mn-Ga-Fe system is plotted as a function of e/a . As can be seen from this plot, data from different families

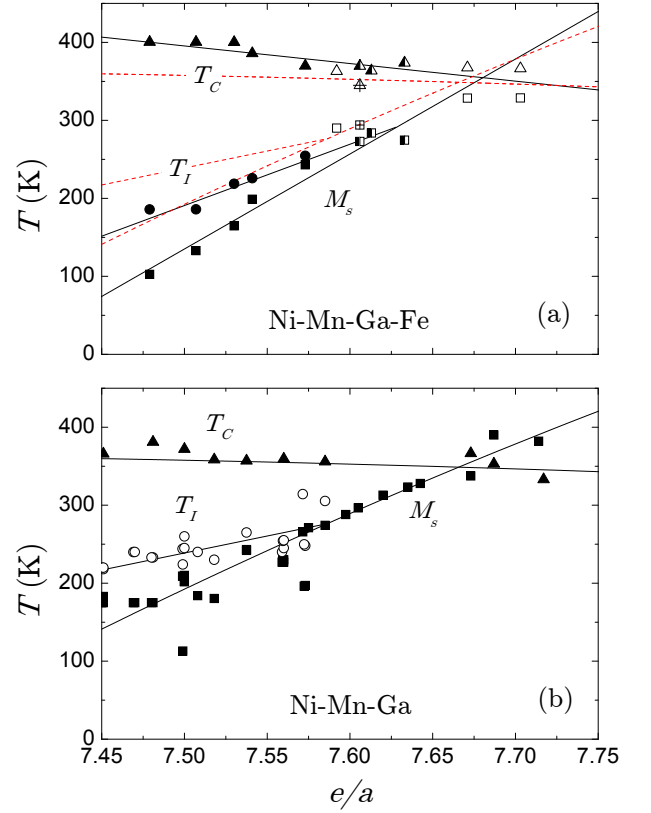


FIG. 7: (Color online) (a) Phase diagram of Ni-Mn-Ga-Fe system as a function of electron concentration per atom e/a . Filled symbols stand for $\text{Ni}_{52.5-x}\text{Mn}_{23}\text{Ga}_{24.5}\text{Fe}_x$ family; half-filled symbols stand for $\text{Ni}_{51.4}\text{Mn}_{25.2-x}\text{Ga}_{23.4}\text{Fe}_x$ family; open symbols stand for $\text{Ni}_{51.4}\text{Mn}_{24.5}\text{Ga}_{24.1-x}\text{Fe}_x$ family; crossed symbols stand for data extracted from reference [26]. Red dashed lines depict the (fitted) transition lines of the related Ni-Mn-Ga ternary system. (b) Phase diagram of Ni-Mn-Ga system as a function of electron per atom concentration e/a (data compiled from reference [35]). Solid lines are fits to the experimental data.

scale with the electron concentration parameter. It was established for Ni-Mn-Ga that the phase stability is controlled by e/a [30, 34]. In the case of the quaternary system, the reasonable scaling of the transition temperatures indicates that the phase stability is mostly governed by the electron concentration as well. However, the scatter in the data points is higher than that observed in the phase diagram as a function of composition (see Figs. 2, 4 and 6), thus suggesting that additional parameters other than electron concentration could affect phase stability.

For comparison, figure 7(b) shows the phase diagram for the Ni-Mn-Ga system (data extracted from reference [35] and references therein). The behavior is similar for both alloy systems. M_s and T_I increase as e/a increases, whereas T_C decreases. At constant e/a , we find that the addition of Fe to Ni-Mn-Ga shifts M_s and T_I to lower values, whereas T_C shifts to higher temperatures [as illustrated by dashed lines in Fig. 7(a)].

The relationship of e/a and lattice instability in cubic

Heusler alloys has recently been investigated from first principles calculations [36]. It has been reported that e/a plays a central role in the occurrence of anomalies in the phonon dispersion curves along [110] directions. These control the stability of the cubic structure. In particular, it has been found that adding and removing electrons has the same effect as replacing the sp (X) element. In the present study, we have experimentally investigated the effect of different element substitution. The general trends in the phase stability are given by the change in e/a . This is consistent with a change in the position of the Fermi energy as in a rigid band model. Nevertheless, the larger scatter of the data when plotted as a function of e/a compared to the one in the plots as a function of composition suggests that the effect of alloying is not just a change in the Fermi level, but the addition of Fe could also modify to some extent the orbital hybridization and bonding. Actually, changes in hybridization were reported for Ni_2MnGa with several substitutional elements [37]. This could be related to volume effects which have been reported for In-doped Ni-Mn-Ga alloys [38].

As can be seen in Fig. 7, the premartensitic phase exists when martensitic and magnetic transition are well separated. In the Ni-Mn-Ga system, it has been shown that magnetoelastic coupling between structural and magnetic degrees of freedom gives rise to the premartensitic transition [11, 39]. The strength of such an interaction depends on the magnetization. Therefore, in order for the premartensitic phase to develop, the sample must remain in the cubic phase at temperatures well below the Curie point. This requires that the martensitic transition temperature is well below T_C . Moreover, the temperature that corresponds to the point where martensitic and premartensitic transformation temperatures meet is slightly displaced to higher e/a values in the case of Ni-Mn-Ga-Fe system with respect to the ternary system. Such a shift is in agreement with the decrease of M_s and the increase of T_C due to Fe addition. As M_s shifts to lower temperatures and T_C to higher temperatures, the separation between both temperatures increases compared to the ternary system for equal e/a values. Thus, the crossing point between M_s and T_I is displaced to higher electron concentration values.

The features in the [110] TA_2 phonon branch giving rise to the intermediate phase are associated with a nesting in the Fermi surface. It has been found that such a Fermi-surface nesting is strongly dependent on the magnetization of the cubic phase [40]. This scenario is consistent with the experimental finding that the premartensitic phase only develops for ferromagnetically ordered samples for which the martensitic instability is well below T_C .

Finally, figure 8 shows the entropy change at the martensitic transformation as a function of electron concentration per atom e/a for (a) Ni-Mn-Ga-Fe and (b) Ni-Mn-Ga systems. As can be seen from panel (a), in the quaternary system ΔS increases as the electron per atom

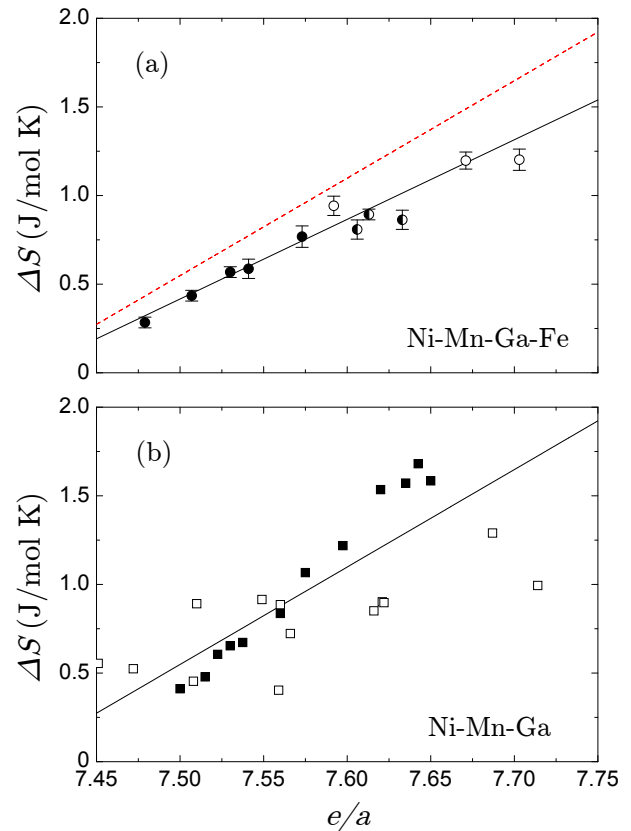


FIG. 8: (Color online) (a) Entropy change at the martensitic transformation of Ni-Mn-Ga-Fe system as a function of electron concentration per atom e/a . Filled symbols stand for $\text{Ni}_{52.5-x}\text{Mn}_{23}\text{Ga}_{24.5}\text{Fe}_x$ family; half-filled symbols stand for $\text{Ni}_{51.4}\text{Mn}_{25.2-x}\text{Ga}_{23.4}\text{Fe}_x$ family; open symbols stand for $\text{Ni}_{51.4}\text{Mn}_{24.5}\text{Ga}_{24.1-x}\text{Fe}_x$ family. Red dashed line depicts the (fitted) entropy change of the related Ni-Mn-Ga ternary system. (b) Entropy change at the martensitic transformation of Ni-Mn-Ga system as a function of electron per atom concentration e/a [data compiled from reference [41] (\square) and [42] (\blacksquare)]. Solid lines are linear fits to the experimental data.

concentration increases, similar to the behaviour exhibited by the martensitic transformation temperatures and to the behaviour of the ternary system. Moreover, the entropy change values in the Fe substituted alloys are lower than those in the ternary Ni-Mn-Ga system, as illustrated by the red dashed line. This drop could be accounted for by the strengthening of magnetic exchange interactions when adding Fe, as reflects the increase of T_C in the quaternary system compared to the ternary one. When magnetic order occurs in the parent phase, the Gibbs chemical free energy decreases, compared to the non magnetic state. Thus, the difference in the free energy between parent and martensite phases is smaller and the parent phase becomes more stable. Actually, the magnetic contribution is also responsible of the strong concentration dependence of the entropy change, as was pointed out by Khovailo *et al.* in the ternary Ni-Mn-Ga system [42].

V. CONCLUSION

We have studied the effect of Fe addition on the structural and magnetic transformation properties in the magnetic shape memory alloy Ni-Mn-Ga for compositions close to stoichiometry. We find that M_s and T_I shift to lower values when Fe is substituted into Ni-Mn-Ga, while T_C shift to higher values. Despite of the similarities between ternary Ni-Mn-Ga and quaternary Ni-Mn-Ga-Fe systems, which indicate that phase stability is qualitatively governed by e/a , the shift in M_s evidences that parameters other than e/a affect phase stability (essentially volume effects associated with atom sizes as suggested in [38]). Hence, a simple choice of e/a can only be considered to be a guideline for examining systematic changes within a single-alloy system. Actually, the lack of universal character of e/a parameterization has been

previously pointed out for the Heusler alloys Ni-Mn-X [33, 43] and has been recently confirmed by the manipulation of structural and magnetic transition temperatures in isoelectronic Ni-Mn-Ga and Ni-Mn-Ga-In compounds [38, 44].

Acknowledgments

This work received financial support from the CI-CyT (Spain), Project No. MAT2007-61200, DURSI (Catalonia), Project No. 2005SGR00969, from the Deutsche Forschungsgemeinschaft (GK277), from Marie-Curie RTN Multimater (Contract No. MRTN-CT-2004-505226), and from CONACYT (44786-SEP-CONACYT 2003). XM acknowledges support from DGICYT (Spain). We thank Peter Hinkel for technical support.

-
- [1] R. C. O'Handley, J. Appl. Phys. **83**, 3263 (1998); O. Söderberg, A. Sozinov, Y. Ge, S.-P. Hannula, and V. K. Lindroos, Handbook of Magnetic Materials, volume 16, edited by J. Buschow, Elsevier Science, Amsterdam (2006).
 - [2] T. Krenke, E. Duman, M. Acet, E. F. Wassermann, X. Moya, L. Mañosa, A. Planes, E. Suard, and B. Ouladdiaf, Phys. Rev. B **75**, 104414 (2007).
 - [3] K. Ullakko, J. K. Huang, C. Kantner, R. C. O'Handley, and V.V. Kokorin, Appl. Phys. Lett. **69**, 1966 (1996).
 - [4] A. Zheludev, S. M. Shapiro, P. Wochner, A. Schwartz, M. Wall, and L. E. Tanner, Phys. Rev. B **51**, 11310 (1995).
 - [5] A. Zheludev, S. M. Shapiro, P. Wochner, and L. E. Tanner, Phys. Rev. B **54**, 15045 (1996).
 - [6] U. Stühr, P. Vorderwisch, V. V. Kokorin, and P.-A. Lindgård, Phys. Rev. B **56**, 14360 (1997).
 - [7] L. Mañosa, A. Planes, J. Zarestky, T. Lograsso, D. L. Schlagel, and C. Stassis, Phys. Rev. B **64**, 024305 (2001).
 - [8] J. Worgull, E. Petti, and J. Trivisonno, Phys. Rev. B **54**, 15695 (1996).
 - [9] L. Mañosa, A. González-Comas, E. Obradó, A. Planes, V. A. Chernenko, V. V. Kokorin, and E. Cesari, Phys. Rev. B **55**, 11068 (1997).
 - [10] M. Stipcich, L. Mañosa, A. Planes, M. Morin, J. Zarestky, T. Lograsso, and C. Stassis, Phys. Rev. B **70**, 054115 (2004).
 - [11] A. Planes, E. Obradó, A. González-Comas, and L. Mañosa, Phys. Rev. Lett. **79**, 3926 (1997).
 - [12] S. R. Barman, S. Banik, and A. Chakrabarti, Phys. Rev. B **72**, 184410 (2005).
 - [13] P. A. Bhobe, K. R. Priolkar, and P. R. Sarode, Phys. Rev. B **74**, 224425 (2006).
 - [14] R. Ranjan, S. Banik, S. R. Barman, U. Kumar, P. K. Mukhopadhyay, and D. Pandey, Phys. Rev. B **74**, 224443 (2006).
 - [15] S. Banik, A. Chakrabarti, U. Kumar, P. K. Mukhopadhyay, A. M. Awasthi, R. Ranjan, J. Schneider, B. L. Ahuja, and S. R. Barman, Phys. Rev. B **74**, 085110 (2006).
 - [16] J. I. Pérez-Landazábal, V. Sánchez-Alarcos, C. Gómez-Polo, V. Recarte, and V. A. Chernenko, Phys. Rev. B **76**, 092101 (1997).
 - [17] B. L. Ahuja, B. K. Sharma, S. Mathur, N. L. Heda, M. Itou, A. Andrejczuk, Y. Sakurai, A. Chakrabarti, S. Banik, A. M. Awasthi, and S. R. Barman, Phys. Rev. B **75**, 134403 (2007).
 - [18] S. Banik, R. Ranjan, A. Chakrabarti, S. Bhardwaj, N. P. Lalla, A. M. Awasthi, V. Sathe, D. M. Phase, P. K. Mukhopadhyay, D. Pandey, and S. R. Barman, Phys. Rev. B **75**, 104107 (2007).
 - [19] Z. H. Liu, M. Zhang, W. Q. Wang, W. H. Wang, J. L. Chen, and G. H. Wu, J. Appl. Phys. **92**, 5006 (2002).
 - [20] V. V. Khovailo, T. Abe, V. V. Koledov, M. Matsumoto, H. Nakamura, R. Note, M. Ohtsuka, V. G. Shavrov, and T. Takagi, Mater. Trans. **44**, 2509 (2003).
 - [21] D. Kikuchi, T. Kanomata, Y. Yamaguchi, H. Nishihara, K. Koyama, and K. Watanabe, J. All. Comp. **383**, 184 (2004).
 - [22] K. Koho, O. Söderberg, N. Lanska, Y. Ge, X. Liu, L. Straka, J. Vimpary, O. Heczko, and V. K. Lindroos, Mater. Sci. Eng. A **378**, 384 (2004).
 - [23] S. Guo, Y. Zhang, B. Quan, J. Li, Y. Qi, and X. Wang, Smart Mater. Struct. **14**, S236 (2005).
 - [24] I. Glavatsky, N. Glavatska, O. Soderberg, S. P. Hannula, and J. U. Hoffmann, Scripta Mater. **54**, 1891 (2006).
 - [25] M. Ohtsuka, M. Matsumoto, and K. Itagaki, Mater. Sci. Eng. A **438**, 935 (2006).
 - [26] F. Hu, B. Shen, J. Sun, and G. Wu, Phys. Rev. B, **64**, 132412 (2001).
 - [27] S. K. Wu, and S. T. Yang, Mater. Lett., **57**, 4291 (2003).
 - [28] R. Tickle, and R. D. James, J. Magn. Magn. Mater., **195**, 627 (1999).
 - [29] V. V. Kokorin, V. A. Chernenko, E. Cesari, J. Pons, and C. Seguí, J. Phys. Condens. Matter **8**, 6457 (1996).
 - [30] V. A. Chernenko, Scr. Mater. **40**, 523 (1999).
 - [31] M. Acet, E. Duman, E. F. Wassermann, L. Mañosa, and A. Planes, J. Appl. Phys. **92**, 3867 (2002).
 - [32] T. Krenke, M. Acet, E. F. Wassermann, X. Moya, L. Mañosa, and A. Planes Phys. Rev. B **72**, 014412 (2005).
 - [33] T. Krenke, M. Acet, E. F. Wassermann, X. Moya, L. Mañosa, and A. Planes, Phys. Rev. B **73**, 174413 (2006).
 - [34] X. Jin, M. Marioni, D. Bono, S. M. Allen, and R. C.

- O’Handley, J. Appl. Phys. **91**, 8222 (2002).
- [35] For Ni-Mn-Ga, data are compiled from a large number of papers. Original references are given in J. Marcos, PhD Thesis, Universitat de Barcelona, Barcelona, 2004.
 - [36] A.T. Zayak, W.A. Adeagbo, P. Entel, K.M. Rabe, Appl. Phys. Lett. **88**, 111903 (2006).
 - [37] J.M. MacLaren, J. Appl. Phys. **91**, 7801 (2002).
 - [38] M. Khan, I. Dubenko, S. Stadler, and N. Ali, J. Phys.: Condens. Matter **16**, 5259 (2004).
 - [39] T. Castán, E. Vives, and P-A. Lindgård, Phys. Rev. B **60**, 7071 (1999).
 - [40] Y. Lee, J.Y. Rhee, B.N. Harmon, Phys. Rev. B **66**, 054424 (2002).
 - [41] V. A. Chernenko, E. Cesari, V. V. Kokorin, and I. N. Vitenko, Scr. metall. mater. **33**, 1239 (1995).
 - [42] V. V. Khovailo, K. Oikawa, T. Abe, and T. Takagi, J. Appl. Phys. **93**, 8483 (2003).
 - [43] T. Krenke, X. Moya, S. Aksoy, M. Acet, P. Entel, L. Mañosa, A. Planes, Y. Elerman, A. Yücel, and E. F. Wassermann, J. Magn. Magn. Mat. **310**, 2788 (2007).
 - [44] S. Aksoy, T. Krenke, M. Acet, E. F. Wassermann, X. Moya, L. Mañosa, and A. Planes, Appl. Phys. Lett. **91**, 241916 (2007).